Chapter 5
Finite Element Modeling and Substructuring to Simulate Shock Plate Testing

Harrison C. Denning, Scott Tuley, Matthew S. Allen, Jeffrey R. Hill, and Daniel R. Roettgen

Abstract Aerospace structures such as rockets can experience various shock events during flight such as stage separation or impacts. These shock events can expose components inside the rocket to large accelerations and stresses which in turn can damage the parts. Shocks are often simulated in the lab using a resonant plate test. This work explores modeling of a 1kHz resonant plate. A shell finite element model is constructed both with and without simple parts attached. Modal transient simulations are used to investigate how many modes are needed to accurately reproduce the response of the plate and part, and the shock response spectrum (SRS) experienced. Then a component, modeled as a single degree-of-freedom system is attached to the center of the plate. The component's mass and fixed-base natural frequency are varied to understand how its SRS is affected.

Keywords Substructuring · Finite Elements · Shock Response

Introduction

Resonant plate and bar tests measure the response of a device under test to shock. The test involves mounting a device onto a large metal plate and striking the opposite side with a projectile to induce vibration. Resonant plate and resonant bar testing have been used to qualify and test aerospace components since their first implementation in the 1980's and 1990's by Davie and Bateman of Sandia National Laboratories [1]. The responses obtained are often represented in shock-response spectra (SRS). While the test is traditionally used to measure the response along a single axis, in more recent years research has looked into how to extend the tests into multiple axis of vibration by changing the location of impact or how the test objects are mounted onto the plate [2, 3, 4, 5].

Most shock tests are designed empirically, with test engineers using a trial and error approach to adjust the parameters of the test (e.g. addition/location of damping bars, location of the test article, programmer material, etc...) until the desired SRS has been obtained. While this is often challenging even for single-axis shock tests, multi-axis testing makes the empirical

Sandia National Laboratories is a multimission laboratory managed and operated by National Technology and Engineering Solutions of Sandia, LLC., a wholly owned subsidiary of Honeywell International, Inc., for the U.S. Department of Energy's National Nuclear Security Administration under contract DE-NA-0003525.

Harrison C. Denning · Scott Tuley
Undergraduate Students, Department of Mechanical Engineering, Brigham Young University, Provo, UT, USA
e-mail: hc.denning22@gmail.com; sttuley@byu.edu

Matthew S. Allen
Professor, Department of Mechanical Engineering, Brigham Young University, Provo, UT, USA
e-mail: matt.allen@byu.edu

Jeffrey R. Hill
Associate Professor, Department of Mechanical Engineering, BYU, Provo, UT, USA
e-mail: dr.jeff.hill@byu.edu

Daniel R. Roettgen
Member of Technical Staff, Sandia National Laboratories, Albuquerque, NM, USA
e-mail: drroett@sandia.gov

Walter D'Ambrogio, et al. (eds.), *Dynamic Substructuring & Transfer Path Analysis, Vol. 4*, Conference Proceedings of the Society for Experimental Mechanics Series, https://doi.org/10.13052/97887-438-0149-8_5

approach a daunting task. Finite element analysis (FEA) has been used to model shock tests and shock loading [6, 7, 8] and has been used in several recent works to model resonant plate tests [3, 4, 9, 10, 11]. Efforts have been made to use predict the SRS of a component in a resonant plate shock test, showing promising results [11, 5]. This work explores the feasibility of using finite element analysis and dynamic substructuring to predict the shock response of a component in a resonant plate shock test.

Experimental dynamic substructuring has received increasing attention in recent years in order to accelerate test and analysis work [12]. Dynamic substructuring allows for accurate modeling of a large system by breaking it into component parts. Each subsystem may be modeled using traditional finite element models or a model may be derived experimentally, depending on the application of interest [13]. Subsystem models can then be assembled to accurately predict the response of the total system, avoiding the need to perform a test on the assembly. Jacobson et al. [5] appear to have been the first to use substructuring to predict the response of a component in a resonant plate shock test. They used LaGrange-Multiplier Frequency Based Substructuring (LM-FBS) to predict and optimize the response of a metal block in a multi-axis shock test. Substructuring allowed them to evaluate 110 possible configurations of their test and select the one that would theoretically produce the best multi-axis SRS. However, they also noted that the substructuring predictions under-predicted most of the resonances, as well as the knee frequency in the SRS, and showed that this was due to the way in which the interface was modeled.

This work seeks to build on those prior works by exploring a few questions. First, how many modes must be accurately modeled to predict the SRS in a resonant plate test? Shock has the potential to excite many modes, and it is unclear how many modes of each subcomponent would need to be measured or modeled in order for substructuring predictions to have adequate accuracy. Second, how sensitive is the SRS of a component to the dynamics of the component itself, as opposed to the dynamics of the resonant plate? It is hoped that the case studies presented here can lay the foundation needed to use modal substructuring to predict the SRS of an arbitrary component in a resonant plate test.

This paper will first review the construction of an accurate model of a resonant plate shock response using FEA. Abaqus will be used to create all FE models presented in this work. A model is constructed and the modes of the plate are computed. A study is performed to determine the mesh density is required to achieve convergence. A MATLAB mathematical model is then constructed to derive the response and hence the shock response spectrum (SRS) of the plate. The model is then interrogated to determine the appropriate number of modes to use in this analysis. This reveals that the SRS is dominated by the symmetric bending modes of the plate, as these are these are the modes most strongly excited by the shock pulse. Higher modes have a minor effect unless the damping is very light.

We then explore the influence of the device under test (DUT) on the shock response spectrum. A single degree-of-freedom (SDOF) system is coupled to the resonant plate at its center using substructuring and the fixed-base resonant frequency of the DUT is varied to see how that affects the SRS. The mass of the DUT is also varied, while keeping the resonant frequency constant, to explore its effect. In general, the SRS on the plate (i.e. at the base of the DUT) changes very little as the parameters of the DUT are varied.

The following section reviews the methods used, in particulars of the finite element model and the analytical solution for the response of a system to an impulsive load. Section presents the results of the various case studies.

Methods

Finite Element Analysis (FEA) software has been used increasingly in the last several years to aid in predicting the shock response of resonant plate and resonant bar tests [3, 9]. For our research, the Abaqus package was utilized to simulate the modes of a 1000Hz resonant plate and these modes were imported into MATLAB to compute the plate's response. The model was then augmented by adding a device under test (DUT), attached to the plate at its center, and the response and SRS computed as various parameters were varied.

Developing the Abaqus Model

A resonant plate test is used in the testing and qualification of parts. Its has proved especially useful in replicating pyroshock environments for aerospace applications. The test is performed by striking a heavy metal plate with a projectile. The force pulse input by the projectile is shaped by placing a "programmer" material between the projectile and plate. The modes of the plate also serve to accentuate certain frequencies in the response. This research is concerned only with the standard case where the impact and the DUT are centered on opposite sides of the plate. Several steps were taken to create an accurate model of this test.

Our plate model was created first without any device under test attached to verify the expected behavior of the plate when subjected to the impact. The model was setup using a standard $508 \times 508 \times 50.8$ mm plate made of 6061 aluminum [4]. No

damping bars or other attachments were added and the damping ratio of the plate was set to 0.02 as this appears to be typical [14]. The model was meshed with linear reduced integration (S4R) shell elements.

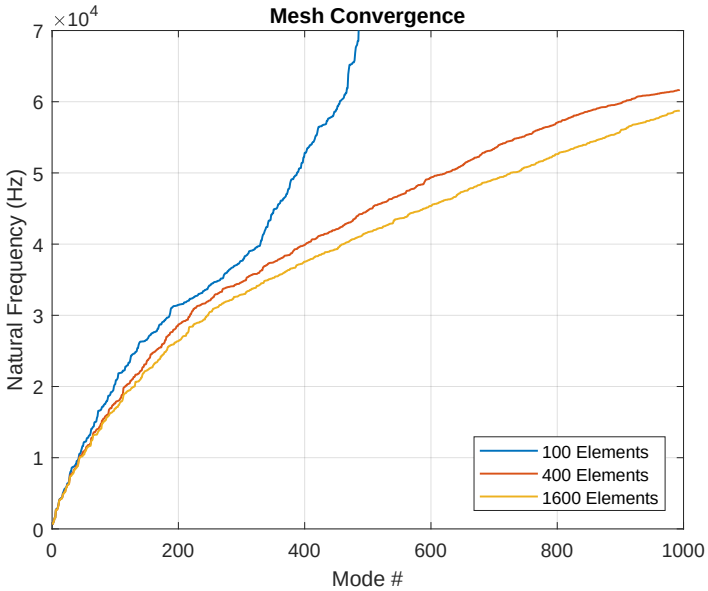

Fig. 1 The natural frequencies computed by Abaqus for three different mesh densities

The appropriate mesh density was determined by comparing the calculated mode frequencies returned by the finite element solver as the mesh density varied. In all cases the square plate was meshed with a uniform grid of hexagonal elements with 10, 20 or 40 elements on a side. Figure 1 shows the frequencies of the first 1000 modes for a plate meshed with 100, 400, and 1600 elements and Figure 2 shows the meshes. The resolution was such that a plate modeled with only 100 elements deviated from the other models after only 50 modes, with an exponential divergence from the other models after 300 modes. When modeled with 400 and 1600 elements, the calculated modes showed a far lesser divergence, although the natural frequencies still differed by about 10^3 Hz after 400 modes or 40kHz. That is most likely beyond the frequency range of interest. All models returned similar values over the first few dozen modes or up to about 10kHz and the modes for the 400 and 1600 element models stayed within 100Hz of one another in that range. This was deemed an acceptable margin and the 400 element model is used for most of the analyses presented subsequently.

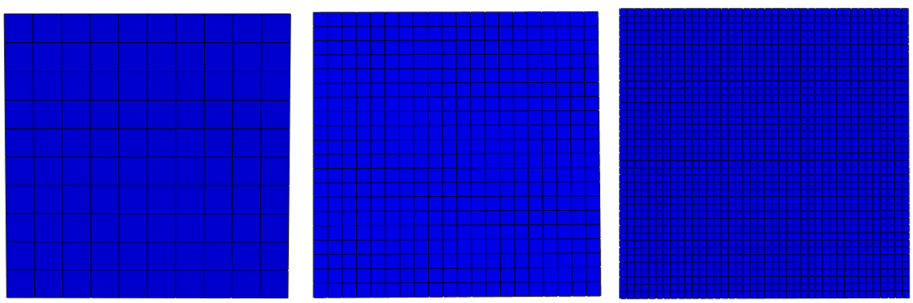

Fig. 2 The three Abaqus models created with 100, 400, and 1600 shell elements

Response of Plate to Impulsive Loading

Figure 3 shows a few of the lower frequency modes of the plate. Abaqus was only used for the initial calculation of mode shapes and frequencies, as it was faster to iterate on the time response in MATLAB. The first 1000 modes were found and imported into MATLAB where the response of the plate was calculated over time. The time response at the center of the plate was used to compute the Shock Response Spectrum (SRS).

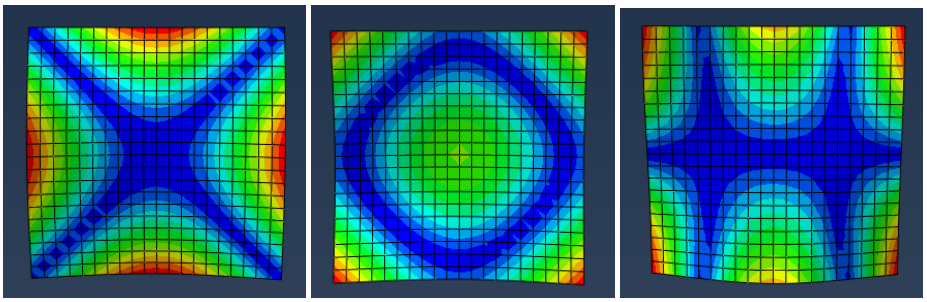

Fig. 3 The Plate as modeled in Abaqus showing several modes, from the top left going clockwise: mode 2 at 912.5 Hz, mode 3 at 1125.4 Hz, and mode 4 at 1538.6 Hz are shown

Once the modes are imported from Abaqus the response of the plate can be solved for using standard solutions for ordinary second order differential equations. The problem is represented by Eq. (1)

$$\mathbf{M}\ddot{\mathbf{x}} + \mathbf{K}\mathbf{x} = \mathbf{F}f_p(t) \tag{1}$$

Where $\mathbf{M}$ and $\mathbf{K}$ are the mass and stiffness matrices, $\mathbf{F}$ represents a vector of zeros with a value of 1 where the force is applied and $f_p(t)$ is the amplitude of the force as a function of time. The force was applied at the center of the plate for all cases considered in this paper. Using the orthogonality properties in Eq. (2) these equations are transformed to the set of uncoupled modal equations in Eq. (3).

$$\boldsymbol{\phi}_j^{\mathrm{T}}[\mathbf{M}]\boldsymbol{\phi}_n = \begin{cases} 0 & \text{if } n \neq j, \\ \mu_j & \text{if } n = j. \end{cases} \qquad \boldsymbol{\phi}_j^{\mathrm{T}}[\mathbf{K}]\boldsymbol{\phi}_n = \begin{cases} 0 & \text{if } n \neq j, \\ \mu_j\omega_j^2 & \text{if } n = j. \end{cases} \tag{2}$$

$$\ddot{\eta}_r + 2\zeta_r\omega_r\dot{\eta}_r + \omega_r^2\eta_r = \boldsymbol{\phi}_r^{\mathrm{T}}\mathbf{F}f_p(t) \tag{3}$$

with $\boldsymbol{\phi}_r^{\mathrm{T}}\mathbf{F}$ being a scalar value. This scalar equation can be solved for each mode of the plate. The solutions are then finally converted back to the original coordinates by using the following.

$$\mathbf{x} = [\boldsymbol{\Phi}]\boldsymbol{\eta} \tag{4}$$

This model was initially solved using a perfect impulse, i.e. $f_p(t) = F_0\delta(t)$ to excite the plate, with an amplitude of $F_0 = 100$ N-s. The solution for each mode is given in Eq. (5), where $\omega_{dr} = \omega_r\sqrt{1-\zeta_r^2}$.

$$\eta_r = \frac{F_0\boldsymbol{\phi}_r^{\mathrm{T}}\mathbf{F}}{\omega_{dr}}e^{-\zeta_r\omega_r t}Re(-ie^{i\omega_{dr}t}) \tag{5}$$

The response was calculated using several different numbers of modes and the SRS was plotted and is shown in Fig. 4. As can be seen, the SRS does not converge to a single SRS as the number of modes increased. As more modes are added the SRS increases and the knee frequency in the curves moves to higher and higher frequencies. This is not an accurate representation of the response that is measured in these types of resonant plate tests. In practice a certain resonant plate typically has a single knee frequency that is centered on the frequency of the first symmetric mode of the plate.

The prior simulations reveal that the shape of the input pulse, and in particular its frequency content are instrumental in setting the knee frequency in an SRS. Cisemore and Babuska [14] showed that sinusoidal and haversine pulses all exhibited a similar SRS, implying that the shape of the pulse was not as important as its bandwidth, so the input force was modeled as a half sine pulse of varying duration $f_p(t) = F_0 sin(\omega_p t)$ for $0 < t < \pi/\omega_p$, because it has a simple analytical solution [15].

The force was once again was applied at the center of the plate and the duration was set to $t_p = \pi/\omega_p$ where $\omega_p = 1000 * 2\pi$. The response of a single mode to this input is given in Eq. (6) for the rth mode. Note that this solution assumes that $\omega_p \neq \omega_r$. The authors actually found that it loses accuracy if $\omega_p \approx \omega_r$, so one must use care to avoid the case where any natural frequency is equal to the pulse frequency ω_p.

$$\eta_r(t) = \frac{F_0\Phi^T\mathbf{F}}{((\omega_r^2-\omega_p^2)^2 + 4\zeta_r^2\omega_r^2\omega_p^2)}\mathrm{Re}[A_{1r}e^{i\omega_p t} + A_{2r}e^{-\zeta_r\omega_r t}e^{i\omega_{dr}t}] \tag{6}$$

where A_{1r} and A_{2r} are

$$A_{1r} = -2\zeta_r\omega_r - i(\omega_r^2 - \omega_p^2) \tag{7}$$

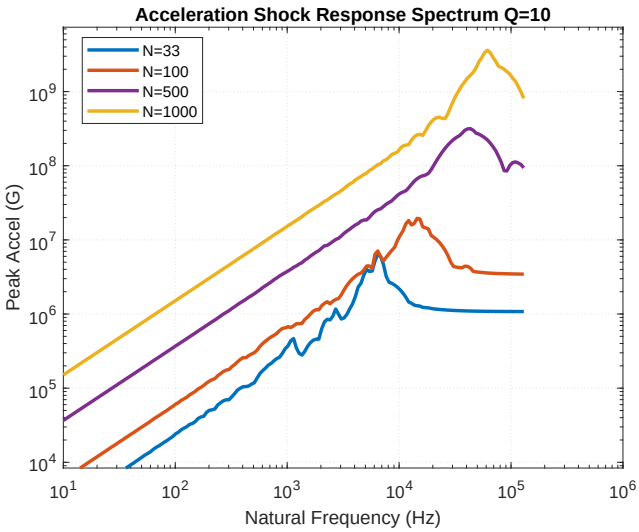

Fig. 4 The SRS of the resonant plate in response to a pure impulse input $f_p(t) = F_0\delta(t)$ as calculated using different numbers of modes

$$A_{2r} = -2\zeta_r\omega_r\omega_p + i\frac{\omega_p(1-2\zeta_r^2)\omega_r^2 - \omega_p^2}{\omega_r\sqrt{1-\zeta_r^2}} \tag{8}$$

This solution holds for the entirety of the forced response or for $0 < t < t_p$, the final state of the forced response at $t = t_p$ is then used as the initial conditions ($\dot{\eta}_r(0)$ & $\eta_r(0)$) and the subsequent response is given by Eq. 9

$$\eta_r = e^{-\zeta_r\omega_r t}\text{Re}[A_{3r}e^{i\omega_{dr}t}] \tag{9}$$

where A_{3r} is

$$A_{3r} = \eta_r(0) - i\frac{\dot{\eta}_r(0) + \zeta_r\omega_r\eta_r(0)}{\omega_{dr}} \tag{10}$$

Again the results are converted back to the original coordinate system using Eq. (4). The SRS was then computed and compared as the number of modes used and frequency of the half sine wave's input was varied. The results are shown in Fig. 5.

SRS plots have become standard in characterizing shock response and were generated for each test run. Their use began with Biot's application of SRS in the analysis of earthquake vibrations but they have since proved useful in analyzing shock and vibrations in many areas of research [16]. An SRS is the maximum acceleration response of an SDOF system whose base input is the shock signal. This is repeated for an SDOF system whose natural frequency is equal to each frequency in the spectrum of interest. Hence, it gives the worst case response of a family of components to the shock input [14]. All of the SRSs presented here where created using the tool provided by Irvine on https://www.vibrationdata.com/, which implements the Smallwood Algorithm with some modifications [17, 18]. For a more detailed mathematical derivation of the algorithm see [19].

When the input frequency of the pulse was kept at or below the plate's resonance a single knee frequency emerged, located at 1140Hz. In those cases (i.e. $\omega_p = 500$ or 1000 Hz), as more modes were added more peaks were observed after the knee, yet the SRS remained more or less at the same level. In contrast, when the higher frequency $\omega_p = 5000$ Hz input was applied, the SRS continued to rise after 1140 Hz and a new knee frequency emerged at 5120 Hz. The simulation failed to capture this effect when only 5 modes were used in the computation. This issue was found to become more prevalent as more modes were included in the computation or when a shorter (or higher frequency) pulse was applied to the system. While not shown here, these were also found to become more pronounced if the damping in the plate was lower.

These results, when taken in conjunction with those in Fig. 4, explain why the SRS did not converge when a perfect impulse was used. The response of the plate is governed by the relatively small number of modes that can be excited by an input at the center. Figure 6 shows the shapes of the first two symmetric modes of the plate; all of the other modes that appear below 5kHz for this plate are anti-symmetric and hence have node lines at the center. If the impulse has infinite bandwidth, then as more modes are added to the simulation the SRS continues to increase, with the knee frequency appearing near the

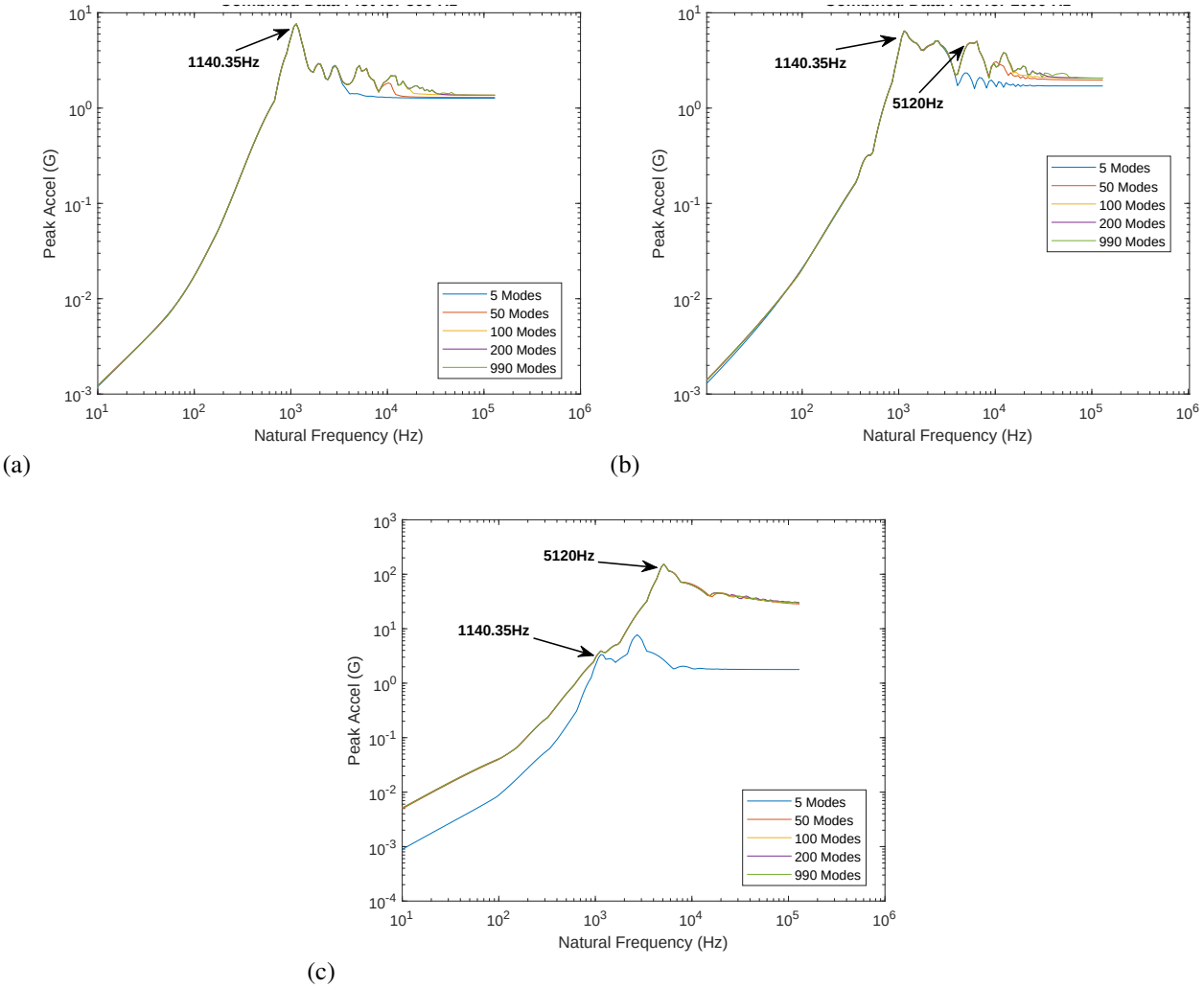

Fig. 5 SRS of the center of the plate, computed using pulse frequencies ω_p= 500, 1000, 5000 Hz in (a), (b) and (c) respectively and with various numbers of modes included in the computation.

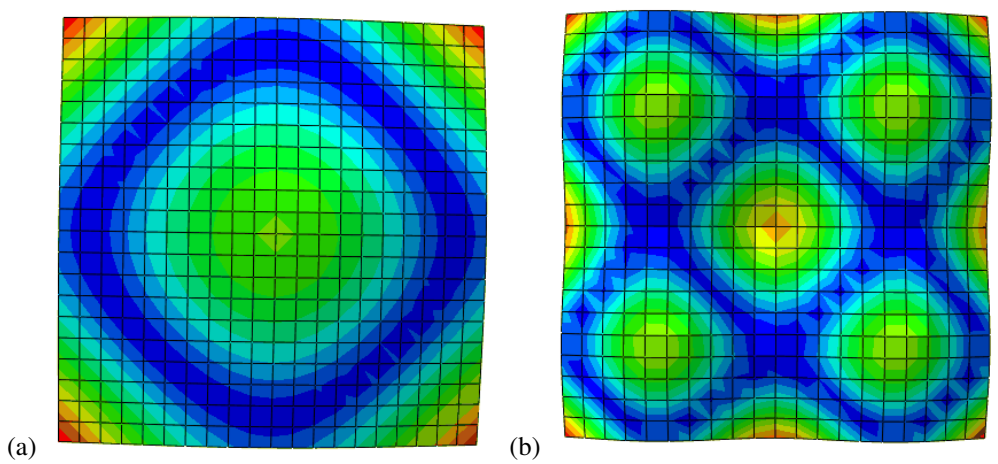

Fig. 6 Mode Shapes of (a) Mode 2 at 1125.4 Hz and (b) Mode 19 at 5067.5Hz. These are the closest modes to the frequencies indicated in Fig. 5.

frequency of the highest frequency mode that was both excited and included in the simulation. In contrast, if the bandwidth of the pulse is limited, then it excites all modes up to a certain frequency and the highest frequency symmetric plate mode dominates the response and produces the knee in the SRS. This behavior explains why a resonant plate test is able to produce a consistent SRS. The ”programmer” material on the back of the plate reduces the bandwidth of the input force, but it is difficult to control the pulse width precisely. These simulations show that the overall response is relatively insensitive to the force pulse width, because the plate accentuates the response, producing a knee near its fundamental breathing mode for a fairly wide range of input forces.

To investigate the effects of damping on the SRS of the plate, the simulations were repeated with varying levels of damping applied to the plate's modes and the results are shown in Figure 7. A higher damping in the plate has a tendency to smooth out the response beyond the knee frequency. This makes the simulations less sensitive to errors in the FE model. While Fig. 1 showed that the high freuqency modes were more sensitive to mesh density, these modes have little effect on the SRS if the damping is high. Once the response of the plate was verified, attention turned to the influence that a component would have on the plate.

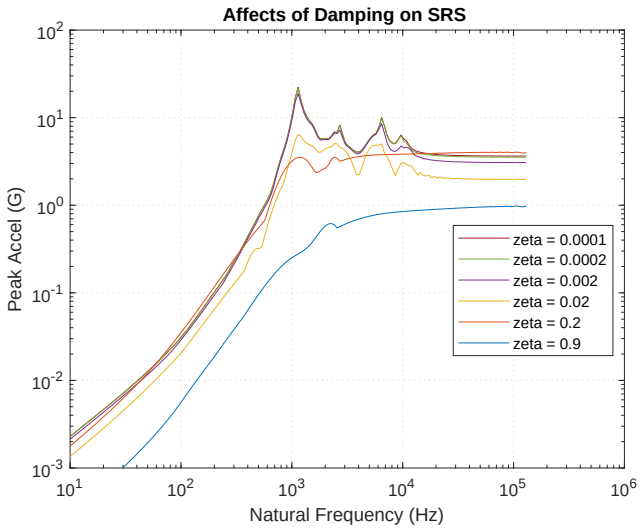

Fig. 7 The SRS of a plate with different levels of damping when subjected to a 0.5msec pulse width. The same damping ratio was applied to all 50 modes used in the simulation.

Results

Having resolved issues of convergence and establishing a workable model of the resonant plate, it was now possible to simulate more complex scenarios. In particular, it was desired to determine how the test article, or component mounted on the plate, changes its SRS. The simplest component could be modeled as a rigid mass, and its effect is already obvious; if the mass is large enough it would lower the natural frequency of the bubble mode and move the knee in the SRS to lower frequencies.

A more realistic component would contain both mass and stiffness. A simple component was modeled as a spring-mass system and was affixed to the plate using the modal model that was imported into MATLAB. The addition of the spring-mass system was achieved using the method of primal assembly. This involves creating a connectivity matrix between the equations of motion of the plate and those of the mass-spring system to be added. The two are linked together with a set of constraints. (For a more detailed derivation see [13]).

The resulting response of the plate was then simulated for various test cases. The plate's response was favored over the component's as the main interest was to analyze how the addition of component to the plate would affect the plate's response, and hence the component's base excited shock environment specification. (While the SRS on the component is not shown here, in general it was observed that the component's SRS closely matched that of the plate including a similar or identical knee but at a higher amplitude. The component's SRS was generally no more than 5g's higher than that of the plate.) It was hypothesized that the component would have the greatest effect on the plate's response when its own resonant frequency matched that of the plate and when it's mass was the highest. Since the exact mass and spring constant values of

the component will vary widely from case to case, the plate's response was simulated as the parameters of the component were varied over a wide range, as shown in Table 1.

Table 1 The mass and spring constant of the component attached to the plate were varied to maintain a given resonant frequency relative to that of the first bubble mode of the plate. The mass was set to be a fraction of the bare plate's 35.4 kg mass. The knee frequencies listed are those observed in Fig. 8.

Component Resonant Freq (Hz)	Mass (kg)	Spring Constant (N/m)	Observed Knee Freq. (Hz)
112.53	35.4×10^{-1}	1.80×10^{6}	1140.35
	35.4×10^{-2}	1.80×10^{5}	1140.35
	35.4×10^{-3}	1.80×10^{4}	1140.35
1125.3	35.4×10^{-1}	1.80×10^{8}	1436.75
	35.4×10^{-2}	1.80×10^{7}	1140.35
	35.4×10^{-3}	1.80×10^{6}	1140.35
11253	35.4×10^{-1}	1.80×10^{10}	1015.94
	35.4×10^{-2}	1.80×10^{9}	1140.35
	35.4×10^{-3}	1.80×10^{8}	1140.35
N/A	0	0	1140.35

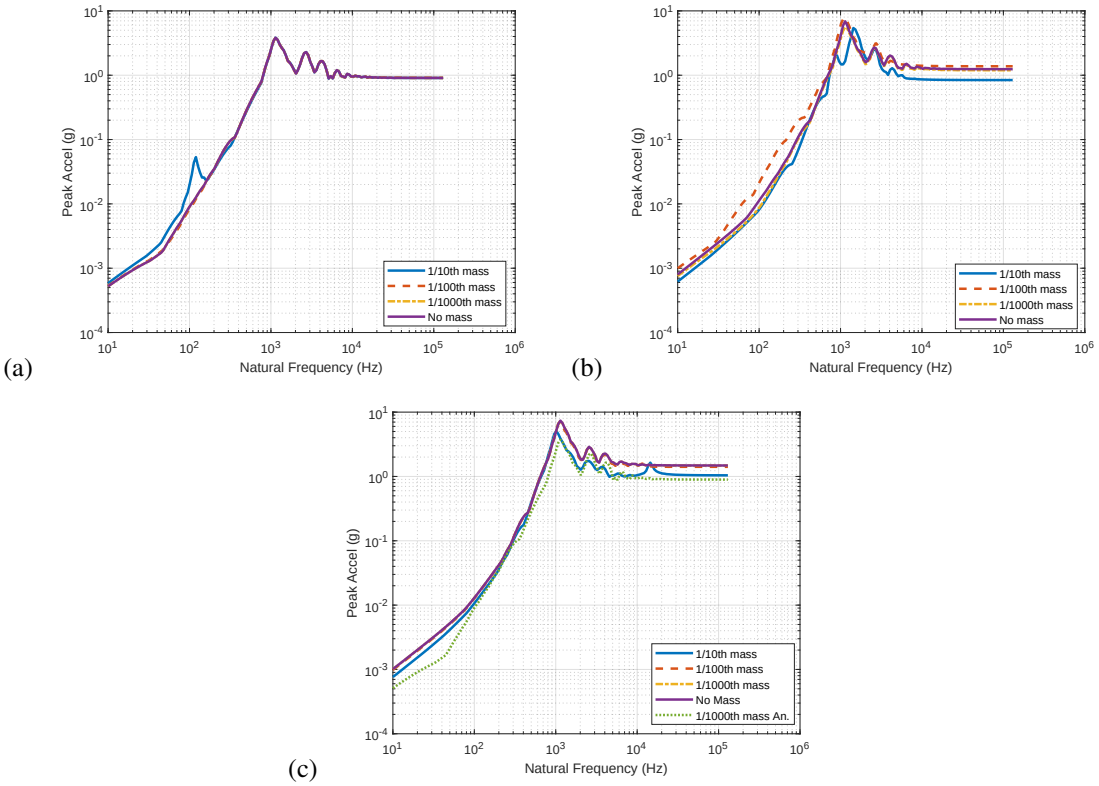

Fig. 8 The SRS of the plate with a single component attached. The parameters of the component are defined in Table 1. The component's mass was a set fraction of the plate's mass, as listed in the legend. The fixed-base resonant frequency of the component was (a) 1/10th, (b) equal, (c) 10 times that of the 1125.4 Hz first bubble mode of the plate.

The resonant frequency of the device is specified by its fixed base natural frequency $f_R = \sqrt{k/m}/(2\pi)$, or the frequency that the component would have if its base was fixed. Note that, to simplify the implementation with the tools available, the component was actually modeled as a 2DOF system consisting of two masses connected by a spring of stiffness k. The mass at the base was given a value of $m/100$ so that the component's mass m is the only important factor. For a particular resonant

frequency the component's mass was then varied between 1/10th, 1/100th, and 1/1000th of the plate's base mass. The spring constant was adjusted accordingly to maintain the desired resonance of the device (see Table 1). The resonant frequency of the device was set at three values: 1/10th the resonant frequency of the plate, at resonance and at 10 times the resonant frequency. The simulations were run with a $\omega_p = 1000$ Hz sine pulse input and are shown in Fig. 8. Note, however, that the cases in Fig. 8(c) were computed with MATLAB's ode45 function. This was necessary because the natural frequency of the plate was nearly 1000 Hz in the case where the component mass was 1/10th of the plate mass, so the analytical formula gave an inaccurate result. The three curves shown were computed with ode45, and the analytical solution for the 1/100th mass case is also shown, confirming that the ode45 settings (RelTol=$1e-9$, AbsTol=$1e-12$) were adequate to produce a solution that agrees reasonably well with the analytical one.

The behavior observed in Fig. 8 is mostly as one might expect. When the component has a low natural frequency, as in Fig. 8(a), the assembly basically has the modes of the plate plus one mode where the component bounces on the approximately rigid plate. That mode occurs at 119 Hz for the case where the component has 1/10th of the plate mass, and it causes a peak that, while visible in the SRS, is not particularly large. For the other cases that mode occurs at 114.0 and 112.5 Hz, but the mass is small enough that it does not affect the plate response noticeably. Note, however, that one would see a change in the SRS on the component.

The largest changes occur when the component's natural frequency is equal to the plate's bubble mode frequency, changing the shape of the SRS significantly, especially when the mass is large. When the component's natural frequency is high relative to the bubble mode of the plate, the component basically acts as a rigid mass that lowers the frequency of the bubble mode, shifting the SRS to the left. This shift is noticeable for the 1/10th mass case, but imperceptible for the other cases.

Table 2 The differences between the SRSs in Fig. 8 are quantified in terms of the maximum and RMS differences between each and the reference case where no component is on the plate.

Component Resonant Freq (Hz)	Mass (kg)	max. difference (g)	Root Mean Square (g)
112.53	35.4×10^{-1}	3.059	0.533
	35.4×10^{-2}	3.062	.532
	35.4×10^{-3}	3.063	0.532
1125.3	35.4×10^{-1}	5.237	0.786
	35.4×10^{-2}	1.969	0.324
	35.4×10^{-3}	1.302	0.156
11253	35.4×10^{-1}	3.4856	0.664
	35.4×10^{-2}	0.5556	0.916
	35.4×10^{-3}	0.0544	0.0088
N/A	0	0	0

Conclusion

These results offer some insight into the potential future use of substructuring techniques to simulate resonant plate tests. The simulations show that the force pulse width must be chosen in conjunction with the resonant plate's bubble mode frequency to obtain the typical SRS with a knee at 1kHz. (The force pulse width is set by the programming material on the back of the plate.) When this is done, the SRS is dominated by a single mode - the bubble mode, which was at 1125 Hz for the plate studied here. On the other hand, if the force pulse bandwidth extends to 5kHz, then a higher order bubble mode can respond and the SRS changes considerably. In that case one must include up to 19 modes at least; convergence was obtained with 50 modes in the simulations shown here. Modes beyond the knee frequency have a minor effect on the SRS.

When a component was added to the resonant plate, it changed the SRS in ways that were fairly straightforward to predict, as discussed in the prior section. The changes were also relatively small, mostly because the component mass was always small relative to the resonant plate. If the fixed-base natural frequencies and mass of the component are known, one can presumably use these results to predict the types of changes that might occur in the SRS.

Future work will build on these results, addressing cases where the component has both mass and inertia and interfaces with the resonant plate over a non-negligible area. (In the simulations presented here, the component was modeled as a point mass connected at the exact center of the plate.)

References

1. Davie, N.T. and Bateman, V.I. “Recent developments in phyroshock simulation using fixtures with tunable resonant frequencies”. Technical Report SAND-94-0350C, Sandia National Labs (1994)
2. Soine, D.E., Schoenherr, T.F., and Bouma, A.J. “Resonant bar shock test equipment under offset loading”. In Schoenherr, T., Karlicek, A., and Beale, D., editors, *Dynamic Environments Testing, Vol. 7: Proceedings of the 42nd IMAC, A Conference and Exposition on Structural Dynamics 2024*, pages 79–84, Cham (2024) Springer Nature Switzerland.
3. Bouma, A.J., Schoenherr, T.F., and Soine, D.E. “Fixture design and analysis for multi-axis mechanical shock testing”. In *Society for Experimental Mechanics Annual Conference and Exposition*, pages 121–124. Springer (2023)
4. Soine, D.E., Schoenherr, T.F., and Heister, J.D. “Evaluation of a multiaxis shock fixture concept”. In *Society for Experimental Mechanics Annual Conference and Exposition*, pages 61–67. Springer (2023)
5. Jacobson, E.M., Blough, J.R., DeClerck, J.P., Van Karsen, C.D., and Soine, D. “Frequency based substructuring on resonant plate”. In *Special Topics in Structural Dynamics & Experimental Techniques, Volume 5: Proceedings of the 38th IMAC, A Conference and Exposition on Structural Dynamics 2020*, pages 327–333. Springer (2021)
6. Qiu, X., Deshpande, V., and Fleck, N. “Finite element analysis of the dynamic response of clamped sandwich beams subject to shock loading”. *European Journal of Mechanics - A/Solids*, 22(6):801–814 (2003)
7. García-Pérez, A., Sorribes-Palmer, F., Alonso, G., and Ravanbakhsh, A. “Overview and application of fem methods for shock analysis in space instruments”. *Aerospace Science and Technology*, 80:572–586 (2018)
8. Fraser, J.S. “Abaqus implementation of a hyperelastic damage model for glass-reinforced polymers under shock and impact loading”. Master’s thesis, The University of Mississippi (2022)
9. Bouma, A.J., Schoenherr, T.F., and Soine, D.E. “Design and analysis of resonant bar fixtures for multi-axis shock response testing”. In *Society for Experimental Mechanics Annual Conference and Exposition*. Springer (2024)
10. Schoenherr, T.F., Soine, D.E., and Witt, B.L. “Experimental modal analysis of a resonant plate during a mid-field pyroshock replication test”. In *Sensors and Instrumentation, Aircraft/Aerospace and Dynamic Environments Testing, Volume 7: Proceedings of the 40th IMAC, A Conference and Exposition on Structural Dynamics 2022*, pages 41–52. Springer (2022)
11. L. Viale, A.F.L.G., A.P. Daga. “Optimization of irregular-shaped resonant plates for pyroshock testing in the aerospace industry”. In *Proceedings of ISMA2024, Leuven, Belgium* (2024)
12. De Klerk, D. *Dynamic Response Characterization of Complex Systems Through Operational Identification and Dynamic Substructuring*. PhD Thesis, Delft University of Technology (2009)
13. Allen, M.S., Rixen, D., Van Der Seijs, M., Tiso, P., Abrahamsson, T., and Mayes, R.L. *Substructuring in Engineering Dynamics: Emerging Numerical and Experimental Techniques*. Springer, CISM International Centre for Mechanical Sciences (2020).
14. Sisemore, C. and Babuška, V. *The science and engineering of mechanical shock*. Springer (2020)
15. Ginsberg, J.H. *Mechanical and structural vibrations: theory and applications*. John Wiley & Sons, New York, 1st edition (2001)
16. Biot, M.A. *Transient oscillations in elastic systems*. PhD thesis, California Institute of Technology (1932)
17. Smallwood, D.O. et al. “An improved recursive formula for calculating shock response spectra”. *Shock and vibration bulletin*, 51(2):211–217 (1981)
18. Ahlin, K. “Shock response spectrum calculation–an improvement of the smallwood algorithm”. In *70th Shock and Vibration Symposium*. SAVIAC (1999)
19. Irvine, T. “Derivation of the filter coefficients for the ramp invariant method as applied to base excitation of a single-degree-of-freedom system” (2013) http://www.vibrationdata.com/ramp_invariant/ramp_invariant_base.pdf [Accessed 2 Oct 2024].